

1 **Functional proteomics reveals that Slr0237 is a SigE-**
2 **regulated glycogen debranching enzyme pivotal for**
3 **glycogen breakdown**

4

5 Haitao Ge^{1*}, Ye Liu³, Dandan Lu^{2*}

6

7 Running title:

8 GlgX1 is necessary for glycogen breakdown

9

10 ¹State Key Laboratory of Molecular Developmental Biology, Institute of
11 Genetics and Developmental Biology, Chinese Academy of Sciences, No.1
12 West Beichen Rd., Beijing 100101, China.

13 ²State Key Laboratory of Crop Stress Adaptation and Improvement, School of
14 Life Sciences, Henan University, Kaifeng, Henan 475004, China

15 ³Science & Technology Department of Sichuan Province, No.39 Xuedao
16 Street, Chengdu, Sichuan 610016, China

17

18 *Corresponding author

19 Haitao Ge, Ph.D.

20 Email: htge@genetics.ac.cn

21

22 Dandan Lu, Ph.D.

23 Email: ludandan@henu.edu.cn

24

25 **ABBREVIATIONS:**

26 *Synechocystis*: *Synechocystis* sp. PCC 6803

27 WT: Wild type

28 F6P: Fructose-6-phosphate

29 FBP: Fructose-1,6-bisphosphate

30 GAP: glyceraldehyde-3-phosphate

31 1,3-BPG: 1,3-Bisphosphoglycerate

32 PCR: Polymerase chain reaction

33 RT-PCR: Reverse transcription-polymerase chain reaction

34 OD: Optical density;

35 OPP: Oxidative pentose phosphorylation

36 ORF: Open reading frame

37 DEPs: differentially expressed proteins

38 Chl: Chlorophyll

39 MS: Mass spectrometry

40 TMT: Tandem mass tag

41 RP-HPLC: Reversed phase-high performance liquid chromatography

42

43 **Significance Statement:**

44 The SigE factor was important role in regulating central carbon metabolism
45 in cyanobacteria. However, the biological processes regulated by SigE remain
46 poorly understood. Proteomics studies showed that SigE depletion induces
47 differential protein expression for sugar catabolic pathways including glycolysis,
48 oxidative pentose phosphate (OPP) pathway, and glycogen catabolism. Two
49 glycogen debranching enzyme homologues Slr1857 and Slr0237 were found
50 differentially expressed in Δ sigE. Biochemistry study indicates that Slr0237
51 plays the major role as the glycogen debranching enzyme in *Synechocystis*.
52 Our study offers new clues for discovering the regulatory mechanism of sugar
53 metabolism in cyanobacteria.

54

55 **Abstracts:**

56 The group 2 σ factor for RNA polymerase SigE plays important role in
57 regulating central carbon metabolism in cyanobacteria. However, the regulation
58 of SigE for these pathways at a proteome level remains unknown. Using a *sigE*-
59 deficient strain ($\Delta sigE$) of *Synechocystis* sp. PCC 6803 and quantitative
60 proteomics, we found that SigE depletion induces differential protein expression
61 for sugar catabolic pathways including glycolysis, oxidative pentose phosphate
62 (OPP) pathway, and glycogen catabolism. Two glycogen debranching enzyme
63 homologues Slr1857 and Slr0237 are found differentially expressed in $\Delta sigE$.
64 Glycogen determination indicated that $\Delta slr0237$ accumulated glycogen under
65 photomixotrophic conditions but was unable to utilize these reserves in the dark,
66 whereas $\Delta slr1857$ accumulates and utilize glycogen in a similar way as the WT
67 strain does in the same conditions. These results suggest that Slr0237 plays
68 the major role as the glycogen debranching enzyme in *Synechocystis*. To our
69 knowledge, this is the first study to report the functional difference of two
70 glycogen debranching enzyme in *Synechocystis* and the research highlights
71 the intricate regulation of glycogen breakdown.

72

73

74

75 **Keywords:** proteomics, SigE, carbon metabolism, glycogen debranching
76 enzyme, *Synechocystis*

77

1 | INTRODUCTION

Cyanobacteria are a group of Gram-negative bacteria that can perform photosynthesis similar to the higher plants. They can use sunlight to fix carbon dioxide in the air through the Calvin cycle and provide energy and carbon sources for cellular metabolism (De Marais, 2000; Kasting & Siefert, 2002). Among the photosynthesis organisms, the unicellular cyanobacterium *Synechocystis* sp. PCC 6803 (hereafter *Synechocystis*) is one of the important model stains that has been widely used for studying photosynthesis and carbon metabolism because it has clear genomic information and is amenable to genetic manipulation (Gao et al., 2014; Kaneko et al., 1996; Vermaas, 1996). *Synechocystis* can grow autotrophically under light conditions and sustain life by breaking down stored carbohydrates such as glycogen in the dark. The glucose-tolerant strain of *Synechocystis* can even utilize exogenous organic carbon to maintain cell growth (Fang et al., 2016; Williams, 1988).

Carbon metabolism is central to cyanobacteria in cooperation with energy and reducing equivalent producing photosynthesis while providing carbon skeleton for synthesis of the other metabolites. In dark, the accumulated carbon reserves such as glycogen can be degraded to supply energy, reducing power, and precursors for biosynthesis of macromolecules necessary for the survival of cyanobacterial cells. Thus, the carbon metabolism needs to be precisely regulated, in both time and space. So far, the expression of genes involved in carbon metabolism was reported to be regulated by multiple proteins such as histidine kinase Hik31 and its plasmid paralog Slr6041 (Kahlon et al., 2006; Nagarajan et al., 2014), the response regulator Rre37 (Tabei et al., 2007), and the Group 2 σ Factor SigE (Osanai et al., 2005). Of these SigE-regulated genes are mainly involved in sugar catabolism as revealed by microarray-based transcriptomics and a targeted proteomics study (Azuma et al., 2011; Osanai et al., 2005). Sugar catabolism in *Synechocystis* cells is roughly divided into glycogen catabolism, Embden-Meyerhof-Parnas pathway (Glycolysis), oxidized pentose phosphate (OPP) pathway, and the tricarboxylic acid (TCA)

108 cycle. A number of the metabolic reactions in these pathways might require the
109 catalysis from enzymes encoded by multiple genes. Some of these reactions
110 are bidirectional while the others are unidirectional. For the bidirectional
111 reactions usually one direction is involved in carbon anabolism and the other in
112 carbon catabolism. Usually multiple isoenzymes are involved in such a
113 bidirectional reaction, with each predominately catalyzing the reaction towards
114 a specific direction. For example, the conversion of glyceraldehyde-3-
115 phosphate (GAP) to 1,3-Bisphosphoglycerate (1,3-BPG), a reaction integral to
116 glycolysis, was reported to be catalyzed by glyceraldehyde 3-phosphate
117 dehydrogenase 1 (GAP1), whereas the conversion of 1,3-BPG to GAP, a
118 reaction involved in gluconeogenesis, was reported to be catalyzed by GAP2
119 (Koksharova et al., 1998). For such bidirectional reactions the enzyme
120 catalyzing the catabolic reactions is more likely regulated by SigE. For the
121 unidirectional multiple isoenzyme-involved reactions, it is conceivable to
122 presume that the one regulated by SigE could play the major role in catalyzing
123 the reaction. Two steps in glycogen breakdown are such unidirectional reaction,
124 one is catalyzed by glycogen phosphorylase (GlgP) and the other is catalyzed
125 by glycogen debranching enzyme (GlgX). Both GlgP and GlgX have two
126 isoenzymes. The difference of functional regulation and specificity of the two
127 isoemzymes of GlgP have been characterized more or less (Fu & Xu, 2006),
128 and SigE is not involved in the regulation of either one. For GlgX, the functions
129 and specificities of the two isoenzyme Slr0237 (GlgX1) and Slr1857 (GlgX2)
130 have not been characterized so far. However, GlgX1 is reported to be regulated
131 by SigE based on the transcriptomics study (Osanai et al., 2005). A reasonable
132 postulation based on this information is that GlgX1 but not GlgX2 is the major
133 glycogen debranching enzyme responsible for glycogen breakdown in
134 *Synechocystis*.

135 Herein, we first generated a *sigE* knockout mutant strain of *Synechocystis*
136 and then quantitatively profiled its proteome in an attempt to systematically
137 identify SigE-regulated proteins. Although SigE-regulated genes have been

138 identified in large scale by microarray-based transcriptomics studies using both
139 *sigE* knockout and overexpressing strains of *Synechocystis*, and by targeted
140 proteomics for a set of 112 proteins (Tokumaru et al., 2018). These studies are
141 not sufficient to comprehensively catalog the SigE-regulated proteins. For the
142 microarray studies, the microarray library only contains 3264 ORFs and 408
143 ORFs harbored by seven endogenous plasmids were not included. The
144 proteins encoded by the plasmid-borne ORFs may be functionally important,
145 particularly in regulation of carbon metabolism, as demonstrated by Slr6041, the
146 paralog of the histidine kinase Hik31 (Nagarajan et al., 2014). Besides, the
147 mRNA level may not be well correlated with protein level as previously reported
148 (Griffin et al., 2002). After confirming that GlgX1 but not GlgX2 is regulated by
149 SigE through the quantitative proteomics, we sought to investigate the distinct
150 role of the two GlgXs, and demonstrated that GlgX1 is the major glycogen
151 debranching enzyme for its breakdown.

152

153 **2 | MATERIALS AND METHODS**

154 **2.1 | Cell Culture**

155 The WT or mutant strains of *Synechocystis* were cultured in liquid BG-11
156 medium in moderate light ($50 \mu\text{mol m}^{-2} \text{s}^{-1}$ photons) in a shaker. The cells were
157 collected by centrifugation (4,000 *g* for 10 min) for biochemical and proteomic
158 analyses at the exponential phase ($\text{OD}_{730 \text{ nm}} = 1.0$). The harvested cells were
159 stored at -80°C until use.

160 **2.2 | Glycogen Content Determination**

161 Glycogen was determined as described (Xu et al., 2013). *Synechocystis* cells
162 were harvested, resuspended in 400 μl 30% (w/v) KOH, and incubated at 95°C
163 for 2 h. Glycogen was then precipitated with 75% (v/v) ice-cold ethanol, pelleted
164 via centrifugation at 10,000 *g* for 10 min, sequentially washed with 70% and 98%
165 (v/v) ethanol, and finally dried at 60°C for 10 min. The isolated glycogen was
166 resuspended in 100 mM sodium acetate (pH 4.5) and enzymatically hydrolyzed
167 to glucose with 2 mg/ml amyloglucosidase (Sigma-Aldrich) at 60°C for 2 h. The

168 glycogen content was determined with a glucose assay kit (Sigma-Aldrich)
169 according to the manufacturer's instructions.

170 **2.3 | Protein Preparation**

171 Cell pellets were lysed in a buffer containing 0.4 M sucrose, 50 mM 3-(N-
172 morpholino) propanesulfonic acid, pH 7.0, 10 mM NaCl, 5 mM EDTA, and 0.5
173 mM phenylmethanesulfonyl fluoride (PMSF, Sigma-Aldrich) with a bead beater.
174 The cell lysates were centrifuged at 4°C to remove insoluble debris (5000 × g,
175 30 min). Total proteins were precipitated with ice-cold 10% trichloroacetic acid
176 in acetone at -20°C, and then washed with acetone. The proteins were then
177 dried with a vacuum and resolubilized with 4% SDS in 0.1 M Tris-HCl, pH 7.6.
178 The protein concentrations were determined using a BCA protein assay kit
179 (Thermo Scientific, Rockford, IL).

180 **2.4 | Protein Digestion and TMT Labeling**

181 Proteins were digested using the filter-aided sample preparation (FASP)
182 method according to a previously described method with slight
183 modifications (Ge et al., 2017; Ge et al., 2018; Wiśniewski et al., 2009). Briefly,
184 the lysates (100 µg protein for each sample) were reduced with 10 mM DTT at
185 37°C for 1 h and alkylated with 55 mM iodoacetamide (IAA, Sigma-Aldrich,
186 Saint Louis, MO) at room temperature for 1 h in the dark. The alkylated lysates
187 were transferred into the Microcon YM-30 centrifugal filter units (EMD Millipore
188 Corporation, Billerica, MA), where the denaturing buffer was replaced by the
189 0.1 M triethylammonium bicarbonate (TEAB, Sigma-Aldrich, Saint Louis, MO),
190 and then digested with sequencing grade trypsin (Promega, Madison, WI) at
191 37°C overnight. The resulting tryptic peptides were collected and labeled with
192 6-plex TMT reagents (Thermo Scientific, Rockford, IL) by incubating peptides
193 with ethanol-dissolved TMT reagents for 2 h at room temperature in dark. The
194 labeling reaction was inactivated by addition of 5% hydroxylamine, and the
195 labeled samples were mixed together with equal ratios before fractionated with
196 reversed phase (RP)-high performance liquid chromatography (HPLC).

197 **2.5 | RP-HPLC**

198 Offline basic RP-HPLC was performed using a Waters e2695 separations
199 HPLC system coupled with a phenomenex gemini-NX 5u C18 column (250 x
200 3.0 mm, 110 Å) (Torrance, CA). The sample was separated with a 97 min basic
201 RP-LC gradient as previously described (Udeshi et al., 2013). A flow rate of 0.4
202 mL/min was used for the entire LC separation. The separated samples were
203 collected into 15 fractions, and completely dried with a SpeedVac concentrator
204 (Thermo Scientific, Rockford, IL) and stored at -20°C for further analysis.

205 **2.6 | Mass Spectrometry Analysis**

206 For MS analysis, the peptides were resuspended in 0.1% formic acid (FA) and
207 analyzed by a LTQ Orbitrap Elite mass spectrometer (Thermo Scientific,
208 Rockford, IL) coupled online to an Easy-nLC 1000 in the data-dependent mode.
209 Briefly, 2 µL of peptide sample (1 µg/µL) was injected into a 15-cm length, 75-
210 µm inner diameter capillary analytic column packed with C18 particles of 5-µm
211 diameter (SunChrom, Friedrichsdorf, Germany). The mobile phases for the LC
212 include buffer A (2% acetonitrile, 0.1% FA) and buffer B (98% acetonitrile, 0.1%
213 FA). The peptides were separated using a 90-min non-linear gradient consisting
214 of 3%-8% B for 10 min, 8%-20% B for 60 min, 20%-30% B for 8 min, 30%-100%
215 B for 2 min, and 100% B for 10 min at a flow rate of 300 nL/min. The source
216 voltage and current were set at 2.5 KV and 100 µA, respectively. All MS
217 measurements were performed in the positive ion mode and acquired across
218 the mass range of 300-1800 m/z. The fifteen most abundant precursor ions
219 from each MS scan were isolated and fragmented by high-energy collisional
220 dissociation (HCD) for MS/MS analysis.

221 **2.7 | Database Search**

222 The raw MS files were searched against the *Synechocystis* proteome sequence
223 database using the software MaxQuant (Cox & Mann, 2008). The database
224 containing 3,672 entries was downloaded from the CyanoBase
225 (<ftp://ftp.kazusa.or.jp/pub/CyanoBase/Synechocystis>, released on 5/11/2009).
226 The type of search was set to report ion MS2 and the 6-plex TMT was chosen
227 for isobaric labels, the minimum reporter parent ion interference (PIF) was set

228 to 0.75. Trypsin was chosen as the protease for protein digestion, and the
229 maximum of 2 was set as the allowable miscleavages. N-terminal acetylation
230 and methionine oxidation were included as the variable modifications. Cysteine
231 carbamidomethylation was chosen as the fixed modification. The mass
232 tolerances were set to 4.5 ppm for the main search and 20 ppm for precursor
233 and fragment ions. The minimum score for unmodified peptides and modified
234 peptides were set to 15 and 40, respectively. Other parameters were set up
235 using the default values. The false discovery rate (FDR) was set to 0.01 for both
236 peptide and protein identifications.

237 **2.8 | Bioinformatics and Statistics**

238 Bioinformatic and statistical analyses were mainly performed using the software
239 Perseus (version 1.6.2.3) (Cox & Mann, 2012) . Student's *t*-test was used to
240 determine the significance of differential expression of proteins between the WT
241 and Δ sigE, and Fisher's-exact test was used for the functional enrichment
242 analysis. A *p*-value<0.05 was used as the cut-off for all statistical analyses.

243 The mass spectrometry proteomics data have been deposited to the
244 ProteomeXchange Consortium via the PRIDE partner repository with the
245 dataset identifier PXD038472 (Perez-Riverol et al., 2022).

246

247 **3 | RESULTS**

248 **3.1 | Disruption of *sigE* in *Synechocystis***

249 Using an insertional mutation approach we generated the *sigE*-deletion mutant
250 (Figure 1A, Left panel) (Gao et al., 2014). An about 2.0-kb spectinomycin
251 resistance gene cassette was inserted into the *sigE* by homologous
252 recombination and the complete segregation of the mutant was confirmed by
253 PCR. Using the same pair of primers for *sigE* ORF fragment amplification which
254 covers the insertion site of the resistance gene cassette, a 1.0-kb and a 3.0-kb
255 PCR products were amplified from the WT and the mutant, respectively,
256 indicating the complete segregation of *sigE* in the mutant (Figure 1A, Right
257 panel). To investigate whether the insertional mutation of *sigE* affects the

258 transcription of its up-or down-stream flanking genes, RT-PCR was used to
259 confirm the transcriptional levels of the ORFs *sll1687*, *sll1688*, *sll1691*, *sll1692*,
260 and *sll1819* which are closely located up- or down-stream of *sigE* (Figure 1B,
261 Left panel). The RT-PCR result (Figure 1B, Right panel) demonstrates that the
262 transcriptional levels of the neighboring ORFs were not affected by the
263 disruption of *sigE*.

264 **3.2 | Depletion of SigE Leads to Impaired Heterotrophic Growth and Dark** 265 **Survival of *Synechocystis***

266 To investigate the effect of *sigE* knockout on the growth of *Synechocystis*, the
267 growth rates of the WT and the mutant were measured in photoautotrophic and
268 mixotrophic conditions under medium light intensity ($50 \mu\text{mol m}^{-2} \text{s}^{-1}$ photons)
269 or in heterotrophic condition in the dark (Figures 2A-B). The results show that
270 there is almost no difference in growth rate between the WT and the ΔsigE
271 cultured in light conditions, except that the mutant strain grew slightly slower
272 than the WT under the photoautotrophic condition (Figure 2A, Left panel).
273 Photographs of the cell cultures at the indicated time points after inoculation
274 show that there is no significant color difference between the two strains under
275 light conditions, indicating that the chlorophyll content was not affected by *sigE*
276 mutation (Figure 2A, Right panel). However, the mutant can hardly grow in dark
277 in the presence of 5 mM glucose, a typical heterotrophic growth condition for
278 *Synechocystis* (Figure 2B). To investigate whether the inhibited growth of the
279 mutant in the heterotrophic condition is due to cell death or repressed
280 proliferation of live cells, the viability of the mutant and the WT in the
281 heterotrophic condition was assayed. The cells were photoautotrophically pre-
282 cultured to the exponential phase ($\text{OD}_{730} = \sim 1.0$), and then incubated in dark
283 up to 96h in the presence or absence of 5mM glucose. The dark-incubated cells
284 were sampled every 24h and spotted onto the solid BG-11 plates, which were
285 subsequently incubated in light for up to 96h and photographed every 24h. The
286 result shows that after 24h-incubation in dark in the presence of glucose, the
287 viability of the mutant was significantly impaired compared with that of the WT

288 as indicated by the inhibited growth of the cells (Figure 2C). After 72h dark
289 incubation, no growth of the mutant was observed indicating all mutants were
290 dead. Instead, the WT cells grew almost equally well compared with those
291 incubated in dark for shorter duration. For the cells dark-incubated without
292 glucose, only minor difference in growth was observed for the WT and the
293 mutant even after 96h dark incubation. Together, these results suggest that
294 viability of the mutant is impaired in the heterotrophic condition, namely the
295 combination of darkness and presence of glucose, but not in dark along, and
296 the latter is worthy of highlighting because the dark viability assay of
297 cyanobacteria has been performed by different reports using or not using
298 glucose (Özkul & Karakaya, 2015), and the consequence is different.

299 **3.3 | Quantitative Identification of Differentially Expressed Proteins in** 300 **Δ sigE**

301 To decipher the proteomic basis of the observed Δ sigE phenotype, a systematic
302 quantitative comparison of the proteomes between the WT and Δ sigE was
303 performed using a 6-plex TMT labeling-based approach (Figure 3). In total,
304 2,193 proteins or protein groups were identified, covering about 60% of the
305 *Synechocystis* proteome (Supplemental Table S1). Grouping the identified
306 proteins according to the functional categories annotated by CyanoBase
307 reveals that identification coverages of all functional categories are higher than
308 50% except for the unknown and other categories (Figure 4A). High coverage
309 identification ensures comprehensive characterization of subsequent
310 quantitative proteomics and bioinformatics analysis.

311 Among all identified proteins 1,925 proteins contain TMT reporter ion
312 intensities (Supplemental Table S2), which were used for further quantification.
313 Student's *t*-test with a threshold $p < 0.05$ was used to filter for 424 proteins
314 quantified with high confidence (Figure 4B), which is indicated by the hierarchy
315 clustering analysis that correctly clustered all three biological replicates of the
316 WT and the mutant. A fold change of 1.4 was used to further filter for the
317 differentially expressed proteins (DEPs) between the two strains, which

318 resulted in 42 upregulated and 95 downregulated proteins in the mutant
319 (Supplemental table S2). Comparisons of the current proteomics data with the
320 transcriptomics data of a previously reported sigE-knockout strain and sigE-
321 overexpressing strain reveal that the differential gene expression patterns at
322 protein and mRNA levels are overall positively correlated between the two sigE-
323 knockout strains (Figure 4C), and is negatively correlated between Δ sigE and
324 the sigE-overexpressing strain (Figure 4D). Nevertheless, a limited number of
325 outliers were also observed such as BioF, Hik37, Amt2, KaiA and FbaA (Figures
326 4C-D), and the inconsistency of differential expression between a mRNA and
327 its protein counterpart is also a well-documented observation (Griffin et al.,
328 2002). In addition, the expression of a number of genes located on the
329 endogenous plasmids of *Synechocystis* was significantly down-regulated in
330 Δ sigE, which was not reported in the transcriptomics data because they were
331 not included in the microarray library (Figures 4C-D; Figure 5).

332 **3.4 | Depletion of SigE Significantly Induces Differential Expression of** 333 **Proteins Involved in Carbon Metabolism**

334 Functional enrichment assay was performed for proteins upregulated or
335 downregulated in Δ sigE using Fisher's exact test. No function was significantly
336 enriched among the upregulated proteins. Manual inspection reveals that some
337 proteins associated with stress responses for *Synechocystis*, such as GgsP,
338 GlpD, sll1483, and sll1863 are upregulated in Δ sigE (Figure 5). Up-regulation
339 of these proteins could implicate SigE in the regulating the acclimation to abiotic
340 stress (Hagemann, 2011), particularly salt and Osmotic stress.

341 Among the downregulated proteins carbon metabolism network and
342 unknown proteins are significantly enriched functional categories (Figure 5;
343 Supplemental Figure 2). In addition, proteins encoded by the genes on the
344 endogenous plasmid pSYSA such as Sll7062, Sll7063, Sll7085, Sll7087, and
345 Sll7089 are also enriched (Figure 5; Supplemental Figure 2). Downregulation
346 of proteins involved in carbon metabolism is consistent with previous
347 observations, whereby depletion of SigE resulted in inhibition of glycolysis, OPP

348 and Glycogen metabolism pathways (Miyuki et al., 2011; Osanai et al., 2005;
349 Tokumaru et al., 2018). Mapping the DEPs to the carbon metabolism network
350 reveals that proteins involved in carbon catabolism but not anabolism were
351 downregulated (Figure 6). This mainly includes Zwf, Gnd, and Tal in the OPP
352 pathway, Gap1, PfkA1, Pyk1, ppsA, and GlgX in the glycolysis and glycogen
353 metabolism pathway (Figures 5-6). Downregulation of these key enzymes in
354 mutant cells indicates that SigE positively regulates sugar metabolism in
355 *Synechocystis*. Among the carbon metabolic pathways a few reactions are
356 bidirectional with one direction for carbon catabolism and the other for carbon
357 anabolism, and each direction is catalyzed by a distinct enzyme. These include
358 the reactions converting Fructose-6-phosphate (F6P) to Fructose-1,6-
359 bisphosphate (FBP) and GAP to 1,3-BPG. Interestingly, the enzymes catalyzing
360 the catabolic direction are downregulated in Δ sigE, underscoring the
361 importance and specificity of SigE in regulating carbon catabolism, and it can
362 be postulated, based on this observation, that a downregulated enzyme
363 involved in carbon metabolism is more likely catalyzing a catabolic reaction.

364 **3.5 | Glycogen Debranching Enzyme Slr0237 (GlgX1) Plays the Major Role** 365 **in Glycogen Breakdown in *Synechocystis***

366 Glycogen debranching is necessary for its breakdown, in *Synechocystis*
367 *slr0237 (glgX1)* and *slr1857 (glgX2)* encode putative isoamylases that
368 debranch glycogen. Previous studies have shown that two transcriptional
369 regulators, SigE and Rre37, regulate the transcriptional expression of *glgX1*
370 and *glgX2*, respectively (Azuma et al., 2011; Osanai et al., 2005). Regulation
371 by different transcription factors indicates that these two GlgXs may play
372 different roles in glycogen metabolism. Down-regulation of GlgX1 in Δ sigE,
373 based on the above assumption, indicates that GlgX1 may play the major role
374 for glycogen debranching and breakdown. To test this hypothesis and to
375 investigate the specific function of the two GlgXs, we generated the knockout
376 mutants for each of the two coding genes (Δ glgX1 and Δ glgX2) in
377 *Synechocystis* by using the insertional mutation method. The completely

378 segregated mutants were confirmed by PCR (Supplemental Figure 1). Growth
379 experiments were performed to determine the effect of the *glgX1* or *glgX2*
380 mutation on cell growth. For photoautotrophic growth, both mutants grew
381 slightly slower than the WT, while the photomixotrophic growth of the two
382 mutants is almost identical with that of the WT (Figures 7A-B, Left panel). The
383 whole cell absorption spectra of the photoautotrophically-growing cells were
384 also measured. Compared with the WT, the spectra of the two *glgX* mutants
385 showed slightly reduced absorption at ~435 nm, ~485 nm, and ~625 nm,
386 indicating slightly lower abundancy of Chl a, carotenoids and phycobilin content,
387 respectively (Supplemental Figure 3). Together, these results suggest that
388 deletion of *glgX* (*slr0237* or *slr1857*) only slightly repressed growth and pigment
389 synthesis of *Synechocystis* under the photoautotrophic condition.

390 In dark, cyanobacteria mainly catabolize glycogen to provide energy,
391 reducing equivalent, and biosynthetic precursors. To investigate the specific
392 functions of the two *GlgX*s in glycogen breakdown, we compared the glycogen
393 breakdown rates of the mutants with that of the WT. The cells were precultured
394 to the exponential phase ($OD_{730} \approx 1$) in the light to allow glycogen accumulation,
395 and then transferred to darkness and incubated for 7 days to boost glycogen
396 breakdown. Seven-day dark-incubation did not cause an apparent change of
397 the cells as indicated by the photographed cultures (Figure 7C). Glycogen
398 contents were measured for cells immediately before and after the dark-
399 incubation. For the cells measured before dark-incubation, there is no
400 significant difference of glycogen contents among the three strains (Figure 7D).
401 For dark-incubated cells, the glycogen contents of WT and Δ *glgX2* were both
402 dramatically reduced, though the amount in Δ *glgX2* is higher than that in the
403 WT. In contrast, the glycogen content of Δ *glgX1* remained almost constant after
404 dark-incubation, indicating glycogen in the mutant was barely catabolized
405 (Figure 7D). Together, these results suggest that *GlgX1* but not *GlgX2* is mainly
406 responsible for glycogen debranching, which is pivotal for glycogen breakdown.

407

408 **4 | DISCUSSION**

409 In the present study, we showed that SigE plays an important role in sugar
410 catabolism and is critical for the dark survival of *Synechocystis* in the presence
411 of glucose. Using a SigE-deficient mutant and quantitative proteomics, we
412 showed that SigE depletion significantly reduced protein expression for sugar
413 catabolic pathways including glycolysis, OPP pathway, and glycogen
414 catabolism.

415 Two glycogen debranching isoenzymes GlgX1 and GlgX2 were found
416 differentially expressed in Δ sigE. Glycogen content determination indicates that
417 Δ glgX1 accumulated glycogen in light but was unable to utilize these reserves
418 in dark. However, Δ glgX2 and WT cells can accumulate and break down
419 glycogen under the same condition. These results indicate that GlgX1 plays the
420 major role as the glycogen debranching enzyme in *Synechocystis*.

421 In *Synechocystis* glycogen is broken down mainly through glycogen
422 phosphorylase (encoded by *glgP*) and glycogen debranching enzyme.
423 *Synechocystis* possesses two *glgP* genes (*sll1356* and *slr1367*) and two *glgX*
424 genes (*slr0237* and *slr1857*) in its genome (Kaneko et al., 1996). Though the
425 specific functions of the two GlgPs have been elucidated (Fu & Xu, 2006), the
426 functional distinction between the two GlgXs is unknown. In this study, we
427 demonstrated that GlgX1 is the major debranching enzyme in glycogen
428 breakdown. The fact that glycogen can be catabolized in Δ glgX2 at a
429 comparable rate with that in the WT suggests that GlgX2 play no or a minor role
430 in glycogen breakdown in *Synechocystis*. Studies in *Escherichia coli* showed
431 that disruption of the *glgX* gene changes the structure patterns of the glycogen
432 produced in cells (Dauvillee et al., 2005). In cyanobacteria, it has also been
433 shown that heterologous expression of *Synechocystis* gene *slr0237* (*glgX1*) or
434 *slr1857* (*glgX2*) in a *glgX* mutant of *Synechococcus elongatus* PCC 7942 (*S.*
435 *elongatus* PCC 7942) could recover the abnormal glycogen structure of mutant
436 cells (Suzuki et al., 2007). When the *glgX1* or *glgX2* gene from *Synechocystis*

437 was introduced to the *glgX* mutant of *S. elongatus* PCC 7942, the level of short
438 branches in the glycogen molecules was significantly reduced in the
439 transformants as compared to the parental mutant. These results indicate that
440 the GlgXs are not only involved in glycogen breakdown but also important for
441 glycogen synthesis by shaping correct glycogen structure.

442 It was also noted that the mutation of *glgX1* and *glgX2* did not cause the
443 over-accumulation of glycogen in *Synechocystis* cells (Figure 7D), the
444 observation was similar to what had been reported for *E. coli* (Dauvillee et al.,
445 2005), *S. elongatus* PCC 7942 (Suzuki et al., 2007) and *Arabidopsis* (Delatte
446 et al., 2006; Wattedled et al., 2005). Although the mutation of *glgX1* and *glgX2*
447 did not cause critical effects on the cellular viability or the growth rate (Figures
448 7A-B), defects in these genes may be disadvantageous in a competitive or
449 stress environment.

450 In *Synechocystis*, both *glgX* genes are significantly induced by nitrogen
451 depletion (Krasikov et al., 2012; Osanai et al., 2006). GlgX1 were decreased by
452 SigE disruption (Osanai et al., 2005) and increased by SigE overexpression
453 (Takashi et al., 2011), whereas GlgX2 were decreased by Rre37 depletion
454 (Azuma et al., 2011). These results indicate that glycogen metabolism could be
455 regulated by distinct mechanisms, particularly under various environmental
456 conditions. In this context, existence of two GlgXs may allow for more flexible
457 regulation of glycogen debranching to better adapt to environmental changes.

458

459 **5 | CONCLUSION**

460 In summary, we found that SigE depletion induces differential protein
461 expression for sugar catabolic pathways especially in glycolysis, OPP pathway,
462 and glycogen catabolism. Two glycogen debranching enzyme homologues
463 Slr1857 and Slr0237 were found differentially expressed in Δ sigE. Glycogen
464 determination indicated that Slr0237 plays the major role as the glycogen
465 debranching enzyme in *Synechocystis*. Our study reports the functional
466 difference of two glycogen debranching enzyme in *Synechocystis* and

467 highlights the intricate regulation of glycogen breakdown in Cyanobacteria.

468

469 **ACKNOWLEDGMENTS:**

470 The work was supported by a grant from National Natural Science Foundation of China

471 (32170253), and a grant from National Key R&D Program of China (2021YFA0909600).

472

473 **CONFLICTS OF INTEREST:**

474 The authors declare no conflict of interest.

475

476 **DATA AVAILABILITY STATEMENT:**

477 The mass spectrometry proteomics data have been deposited to the ProteomeXchange

478 Consortium and can be downloaded at:

479 <http://proteomecentral.proteomexchange.org/cgi/GetDataset>, with the dataset identifier

480 PXD038472

481

482

483 **REFERENCES**

- 484 Azuma, M., Osanai, T., Hirai, M. Y., & Tanaka, K. (2011). A response regulator Rre37 and an RNA
485 polymerase sigma factor SigE represent two parallel pathways to activate sugar
486 catabolism in a cyanobacterium *Synechocystis* sp. PCC 6803. *Plant Cell Physiol*, *52*(2), 404-
487 412. <https://doi.org/10.1093/pcp/pcq204>
- 488 Cox, J., & Mann, M. (2008). MaxQuant enables high peptide identification rates, individualized
489 p.p.b.-range mass accuracies and proteome-wide protein quantification [Evaluation
490 Studies
491 Research Support, Non-U.S. Gov't]. *Nature Biotechnology*, *26*(12), 1367-1372.
492 <https://doi.org/10.1038/nbt.1511>
- 493 Cox, J., & Mann, M. (2012). 1D and 2D annotation enrichment: a statistical method integrating
494 quantitative proteomics with complementary high-throughput data. *BMC Bioinformatics*,
495 *13 Suppl 16*, S12. <https://doi.org/10.1186/1471-2105-13-S16-S12>
- 496 Dauvillee, D., Kinderf, I. S., Li, Z., Kosar-Hashemi, B., Samuel, M. S., Rampling, L., . . . Morell, M. K.
497 (2005). Role of the *Escherichia coli* glgX gene in glycogen metabolism. *J Bacteriol*, *187*(4),
498 1465-1473. <https://doi.org/10.1128/JB.187.4.1465-1473.2005>
- 499 De Marais, D. J. (2000). Evolution. When did photosynthesis emerge on Earth? [Comment]. *Science*,
500 *289*(5485), 1703-1705. <http://www.ncbi.nlm.nih.gov/pubmed/11001737>
- 501 Delatte, T., Umhang, M., Trevisan, M., Eicke, S., Thorneycroft, D., Smith, S. M., & Zeeman, S. C.
502 (2006). Evidence for distinct mechanisms of starch granule breakdown in plants. *J Biol*
503 *Chem*, *281*(17), 12050-12059. <https://doi.org/10.1074/jbc.M513661200>
- 504 Fang, L., Ge, H., Huang, X., Liu, Y., Lu, M., Wang, J., . . . Wang, Y. (2016). Trophic Mode-Dependent
505 Proteomic Analysis Reveals Functional Significance of Light-Independent Chlorophyll
506 Synthesis in *Synechocystis* sp. PCC 6803. *Mol Plant*.
507 <https://doi.org/10.1016/j.molp.2016.08.006>
- 508 Fu, J., & Xu, X. (2006). The functional divergence of two glgP homologues in *Synechocystis* sp. PCC
509 6803. *FEMS Microbiol Lett*, *260*(2), 201-209. <https://doi.org/10.1111/j.1574-6968.2006.00312.x>
- 511 Gao, L., Shen, C., Liao, L., Huang, X., Liu, K., Wang, W., . . . Wang, Y. (2014). Functional Proteomic
512 Discovery of Slr0110 as a Central Regulator of Carbohydrate Metabolism in *Synechocystis*
513 sp. PCC6803. *Molecular & Cellular Proteomics*, *13*, 204-219. <https://doi.org/10.1074/>
- 514 Ge, H., Fang, L., Huang, X., Wang, J., Chen, W., Liu, Y., . . . Wang, Y. (2017). Translating Divergent
515 Environmental Stresses into a Common Proteome Response through Hik33 in a Model
516 Cyanobacterium. *Mol Cell Proteomics*. <https://doi.org/10.1074/mcp.M117.068080>
- 517 Ge, H., Fang, L., Huang, X., Wang, J., Chen, W., Zhang, Y., . . . Wang, Y. (2018). Activation of the
518 Oxidative Pentose Phosphate Pathway is Critical for Photomixotrophic Growth of a hik33-
519 Deletion Mutant of *Synechocystis* sp. PCC 6803. *Proteomics*, *18*(20), e1800046.
520 <https://doi.org/10.1002/pmic.201800046>
- 521 Griffin, T. J., Gygi, S. P., Ideker, T., Rist, B., Eng, J., Hood, L., & Aebersold, R. (2002). Complementary
522 profiling of gene expression at the transcriptome and proteome levels in *Saccharomyces*
523 *cerevisiae*. *Mol Cell Proteomics*, *1*(4), 323-333. [https://doi.org/10.1074/mcp.m200001-
524 mcp200](https://doi.org/10.1074/mcp.m200001-mcp200)
- 525 Hagemann, M. (2011). Molecular biology of cyanobacterial salt acclimation. *FEMS Microbiol Rev*,
526 *35*(1), 87-123. <https://doi.org/10.1111/j.1574-6976.2010.00234.x>

527 Kahlon, S., Beeri, K., Ohkawa, H., Hihara, Y., Murik, O., Suzuki, I., . . . Kaplan, A. (2006). A putative
528 sensor kinase, Hik31, is involved in the response of *Synechocystis* sp. strain PCC 6803 to
529 the presence of glucose. *Microbiology (Reading)*, *152*(Pt 3), 647-655.
530 <https://doi.org/10.1099/mic.0.28510-0>

531 Kaneko, T., Sato, S., Kotani, H., Tanaka, A., Asamizu, E., Nakamura, Y., . . . Tabata, S. (1996).
532 Sequence analysis of the genome of the unicellular cyanobacterium *Synechocystis* sp.
533 strain PCC6803. II. Sequence determination of the entire genome and assignment of
534 potential protein-coding regions. *DNA Res*, *3*(3), 109-136.
535 <https://doi.org/10.1093/dnares/3.3.109>

536 Kasting, J. F., & Siefert, J. L. (2002). Life and the evolution of Earth's atmosphere. *Science*, *296*(5570),
537 1066-1068. <https://doi.org/10.1126/science.1071184>

538 Koksharova, O., Schubert, M., Shestakov, S., & Cerff, R. (1998). Genetic and biochemical evidence
539 for distinct key functions of two highly divergent GAPDH genes in catabolic and anabolic
540 carbon flow of the cyanobacterium *Synechocystis* sp. PCC 6803. *Plant Mol Biol*, *36*(1), 183-
541 194. <https://doi.org/10.1023/a:1005925732743>

542 Krasikov, V., Aguirre von Wobeser, E., Dekker, H. L., Huisman, J., & Matthijs, H. C. (2012). Time-
543 series resolution of gradual nitrogen starvation and its impact on photosynthesis in the
544 cyanobacterium *Synechocystis* PCC 6803. *Physiol Plant*, *145*(3), 426-439.
545 <https://doi.org/10.1111/j.1399-3054.2012.01585.x>

546 Miyuki, A., Takashi, O., Masami Yokota, H., & Kan, T. (2011). A response regulator Rre37 and an
547 RNA polymerase sigma factor SigE represent two parallel pathways to activate sugar
548 catabolism in a cyanobacterium *Synechocystis* sp. PCC 6803. *Plant & Cell Physiology*, *52*(2),
549 404-412.

550 Nagarajan, S., Srivastava, S., & Sherman, L. A. (2014). Essential role of the plasmid hik31 operon in
551 regulating central metabolism in the dark in *Synechocystis* sp. PCC 6803. *Mol Microbiol*,
552 *91*(1), 79-97. <https://doi.org/10.1111/mmi.12442>

553 Osanai, T., Imamura, S., Asayama, M., Shirai, M., Suzuki, I., Murata, N., & Tanaka, K. (2006). Nitrogen
554 induction of sugar catabolic gene expression in *Synechocystis* sp. PCC 6803. *DNA Res*,
555 *13*(5), 185-195. <https://doi.org/10.1093/dnares/dsl010>

556 Osanai, T., Kanesaki, Y., Nakano, T., Takahashi, H., Asayama, M., Shirai, M., . . . Tanaka, K. (2005).
557 Positive regulation of sugar catabolic pathways in the cyanobacterium *Synechocystis* sp.
558 PCC 6803 by the group 2 sigma factor sigE. *J Biol Chem*, *280*(35), 30653-30659.
559 <https://doi.org/10.1074/jbc.M505043200>

560 Özkul, K., & Karakaya, H. (2015). Characterisation of an opcA Mutant of the Unicellular
561 Cyanobacterium *Synechocystis* sp. PCC 6803. *Curr Microbiol*, *71*(5), 572-578.
562 <https://doi.org/10.1007/s00284-015-0889-4>

563 Perez-Riverol, Y., Bai, J., Bandla, C., Garcia-Seisdedos, D., Hewapathirana, S., Kamatchinathan, S., . . .
564 Vizcaino, J. A. (2022). The PRIDE database resources in 2022: a hub for mass
565 spectrometry-based proteomics evidences. *Nucleic Acids Res*, *50*(D1), D543-D552.
566 <https://doi.org/10.1093/nar/gkab1038>

567 Suzuki, E., Umeda, K., Nihei, S., Moriya, K., Ohkawa, H., Fujiwara, S., . . . Nakamura, Y. (2007). Role
568 of the GlgX protein in glycogen metabolism of the cyanobacterium, *Synechococcus*
569 *elongatus* PCC 7942. *Biochim Biophys Acta*, *1770*(5), 763-773.
570 <https://doi.org/10.1016/j.bbagen.2007.01.006>

571 Tabei, Y., Okada, K., & Tsuzuki, M. (2007). Sll1330 controls the expression of glycolytic genes in
572 Synechocystis sp. PCC 6803. *Biochem Biophys Res Commun*, 355(4), 1045-1050.
573 <https://doi.org/10.1016/j.bbrc.2007.02.065>

574 Takashi, O., Akira, O., Miyuki, A., Kan, T., Kazuki, S., Masami Yokota, H., & Masahiko, I. (2011).
575 Genetic engineering of group 2 sigma factor SigE widely activates expressions of sugar
576 catabolic genes in Synechocystis species PCC 6803. *Journal of Biological Chemistry*,
577 286(35), 30962.

578 Tokumaru, Y., Uebayashi, K., Toyoshima, M., Osanai, T., Matsuda, F., & Shimizu, H. (2018).
579 Comparative Targeted Proteomics of the Central Metabolism and Photosystems in SigE
580 Mutant Strains of Synechocystis sp. PCC 6803. *Plant Physiology*, 23(5), pp.01711.02017.

581 Udeshi, N. D., Svinkina, T., Mertins, P., Kuhn, E., Mani, D. R., Qiao, J. W., & Carr, S. A. (2013). Refined
582 preparation and use of anti-diglycine remnant (K-epsilon-GG) antibody enables routine
583 quantification of 10,000s of ubiquitination sites in single proteomics experiments.
584 *Molecular and Cellular Proteomics*, 12(3), 825-831.
585 <https://doi.org/10.1074/mcp.O112.027094>

586 Vermaas, W. (1996). Molecular genetics of the cyanobacterium Synechocystis sp. PCC6803-
587 Principles and possible biotechnology applications. *Journal of Applied Phycology*, 8, 263-
588 273.

589 Wattebled, F., Dong, Y., Dumez, S., Delvallé, D., Planchot, V., Berbezy, P., . . . D'Hulst, C. (2005).
590 Mutants of Arabidopsis lacking a chloroplastic isoamylase accumulate phytyglycogen and
591 an abnormal form of amylopectin. *Plant Physiol*, 138(1), 184-195.
592 <https://doi.org/10.1104/pp.105.059295>

593 Williams, J. G. K. (1988). Construction of specific mutations in photosystem II photosynthetic
594 reaction center by genetic engineering methods in Synechocystis 6803. *167C*, 766-778.

595 Wiśniewski, J. R., Zougman, A., Nagaraj, N., & Mann, M. (2009). Universal sample preparation
596 method for proteome analysis. *Nat Methods*, 6(5), 359-362.
597 <https://doi.org/10.1038/nmeth.1322>

598 Xu, Y., Guerra, L. T., Li, Z., Ludwig, M., Dismukes, G. C., & Bryant, D. A. (2013). Altered carbohydrate
599 metabolism in glycogen synthase mutants of Synechococcus sp. strain PCC 7002: Cell
600 factories for soluble sugars. *Metab Eng*, 16, 56-67.
601 <https://doi.org/10.1016/j.ymben.2012.12.002>

602

603

604 **Figure 1** | Generation of *sigE* knockout mutant in *Synechocystis*.
605 **(A)** The diagram depicts the plasmid construct for disrupting the ORF of *sigE*
606 on the genome of the *Synechocystis*.
607 **(B)** The same pair of primers was used to amplify DNA fragments from the WT
608 and the mutant to confirm the complete segregation of the mutant.
609 **(C)** The diagram shows the genomic locus of *sigE* and its neighboring ORFs.
610 **(D)** Transcription of *sigE* and its neighboring ORFs in WT and $\Delta sigE$ was
611 detected via RT-PCR. The gene *rnpB* was used as the internal loading control.

612

613 **Figure 2** | Disruption of *sigE* affects the heterotrophic growth of *Synechocystis*.
614 **(A-B)** Growth curves of the WT and the $\Delta sigE$ were measured in the presence
615 (+G) or absence of 5 mM glucose under $50 \mu \text{mol m}^{-2}\text{s}^{-1}$ light intensity **(A)** or in
616 dark **(B)** (Left panels). The cell cultures were also photographed at the indicated
617 time points during the growth experiment (Right panels).

618 **(C)** Exponentially-growing WT and $\Delta sigE$ cultured in BG-11 with or without 5μ
619 m glucose were transferred to darkness, and then sampled ($10 \mu\text{l}$ each) at the
620 indicated time points during dark-incubation and spotted on solid BG-11 plates.
621 The plates were incubated in continuous light and photographed every 24 hours
622 after inoculation.

623

624 **FIGURE 3** | Schematic representation of the workflow for the quantitative
625 proteomic analysis of the $\Delta sigE$.

626 Total proteins were extracted from the three biological replicates of the WT and
627 the $\Delta sigE$ and digested with trypsin. The tryptic peptides were labeled with 6-
628 plex TMT reagents in the order as indicated. The labeled peptides were mixed
629 together with an equal molar ratio, and separated into 15 fractions with RP-
630 HPLC. The peptides in each fraction were quantitatively analyzed by LC-
631 MS/MS using a LTQ-Orbitrap-Elite mass spectrometer.

632

633 **FIGURE 4** | Quantitative proteomic analysis of the $\Delta sigE$.
634 **(A)** the bar graph shows the coverage of protein identification for all functional
635 categories annotated by CyanoBase.
636 **(B)** Z-scored TMT reporter intensities of 424 proteins after Student's *t*-test
637 ($p < 0.05$) were used for hierarchy clustering analysis to evaluate the
638 reproducibility of the quantitative analysis. The extents of differential protein
639 expression are color-coded and displayed on the scale bars.
640 **(C-D)** Volcano plots shows the comparison of the results in the current
641 proteomic study and previous transcriptomic studies for *sigE* knockout **(C)** and
642 *sigE* overexpression **(D)** strains. The filled circles indicate proteins with
643 significant changes (fold change ≥ 1.40 or ≤ 0.71 , $p < 0.05$) in expression in the
644 current proteomic study. The red and green spots represent genes that were
645 upregulated or downregulated in the indicated transcriptomic studies.

646

647 **FIGURE 5** | DEPs in major functional categories.

648 Volcano plots shows the differentially expressed proteins in $\Delta sigE$. Proteins
649 involved in carbon metabolism (purple), stress response (red), and encoded by
650 endogenous plasmids (blue) are highlighted.

651

652 **FIGURE 6** | Mapping of the DEPs in the $\Delta sigE$ to a protein network for carbon
653 metabolism.

654 The DEPs are indicated by red or green color, which indicate upregulation and
655 downregulation in the $\Delta sigE$, respectively.

656

657 **FIGURE 7** | Phenotypic analysis of $\Delta slr0237$ and $\Delta slr1857$.

658 **(A-B)** Growth curves of the WT and the mutant strains $\Delta slr0237$ **(A)** and
659 $\Delta slr1857$ **(B)** cultured with or without 5 mM glucose under medium light intensity
660 (Left panels). The cultures were also photographed at the indicated time points
661 (Right panels).

662 **(C-D)** The indicate WT and mutant strains were pre-cultured in light to OD_{730}

663 ~1.0, and then transferred to darkness and dark-incubated up to 168h, the
664 cultures were photographed at the indicated time points **(C)**. Bar graph shows
665 the glycogen contents of the WT and the mutants before and after dark-
666 incubation **(D)**.

667

668 **Supplemental Figure 1** | PCR confirmation of the complete segregation of the
669 Δ slr0237 and Δ slr1857.

670 The same pair of primers were used to amplify DNA fragments from the WT
671 and the mutants genomic DNA to confirm the complete segregation of the
672 mutant.

673

674 **Supplemental Figure 2** | Functions enriched in the downregulated proteins in
675 Δ sigE.

676 The gene ontology terms, KEGG pathways, functional categories annotated by
677 the CyanoBase and carbon metabolism network in Figure 6 were included for
678 the analysis. FDR<0.02 and the enrichment factor ≥ 1.5 were used as the cutoffs
679 to include all enriched categories.

680

681 **Supplemental Figure 3** | Whole cell absorbance spectra of Δ slr0237, Δ slr1857
682 and the WT strains.

683 Cells were sampled during the exponential growth phase ($OD_{730} = \sim 0.8$). The
684 absorption spectra was scanned between 380 and 800 nm. The spectra were
685 normalized to the OD_{730} .

686

Figure 1

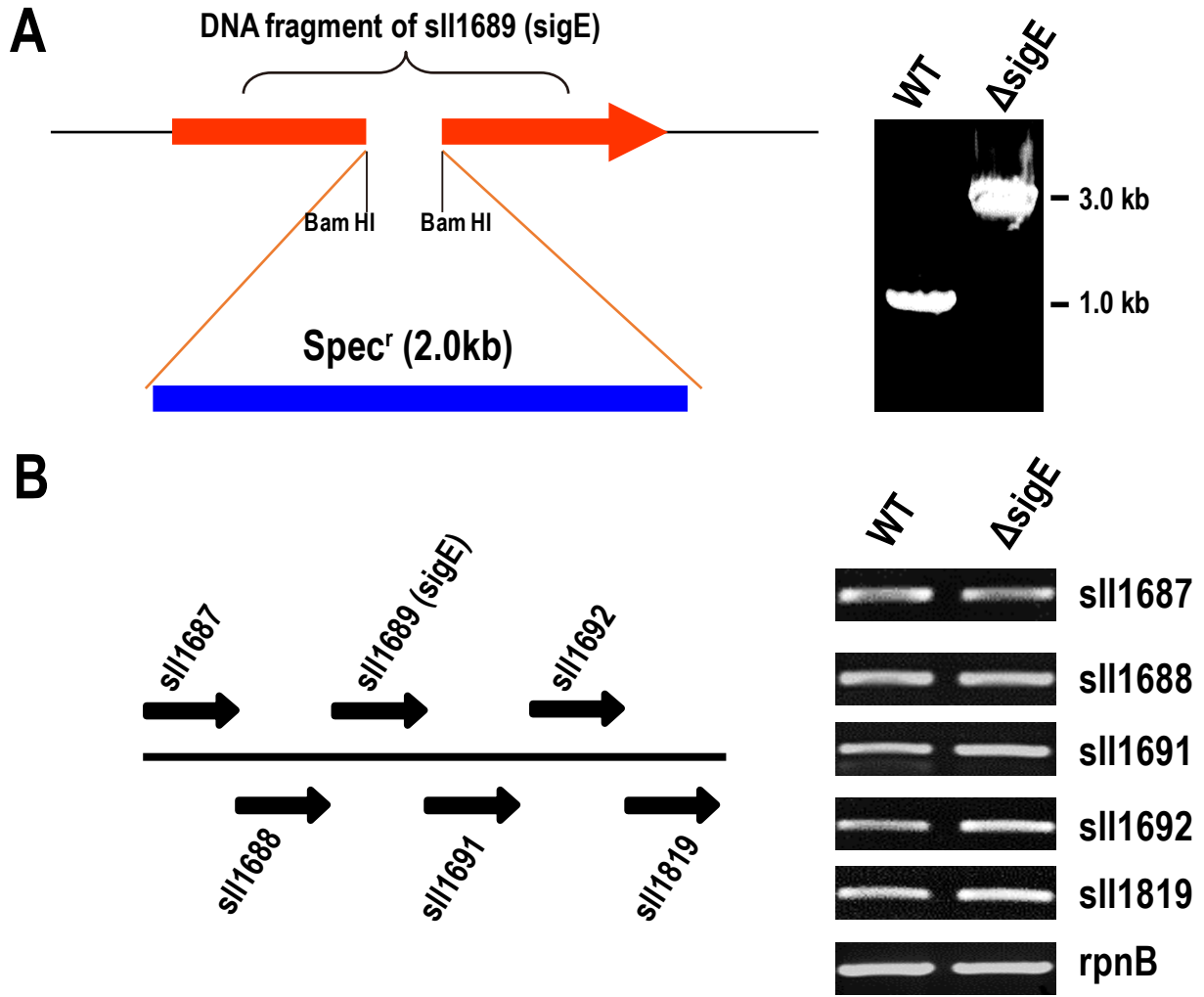
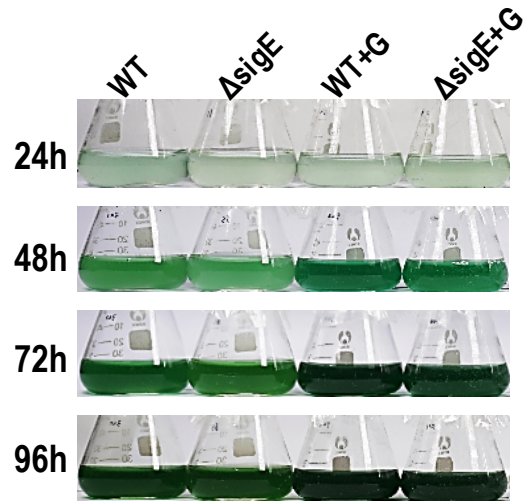
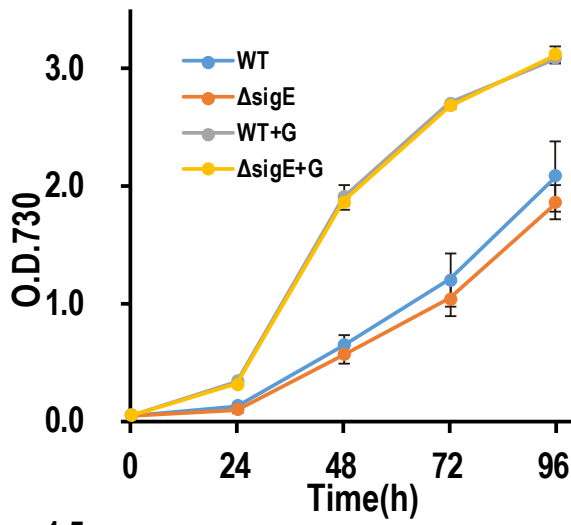
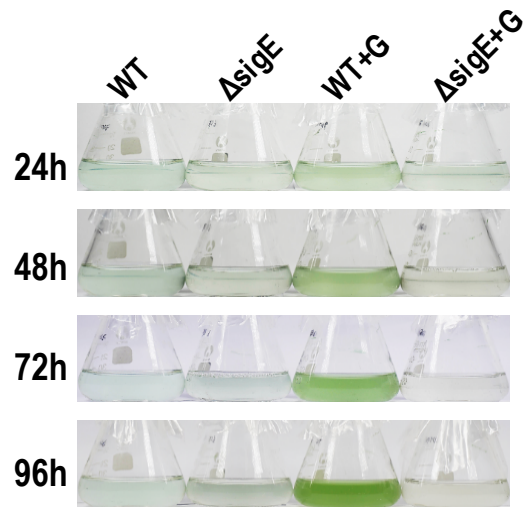
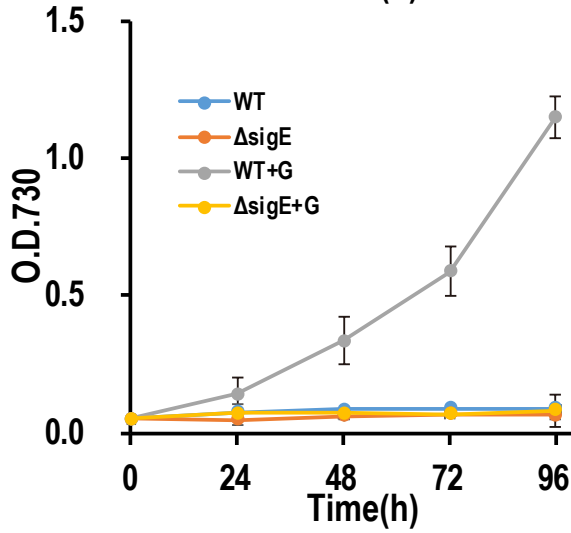


Figure 2

A



B



C

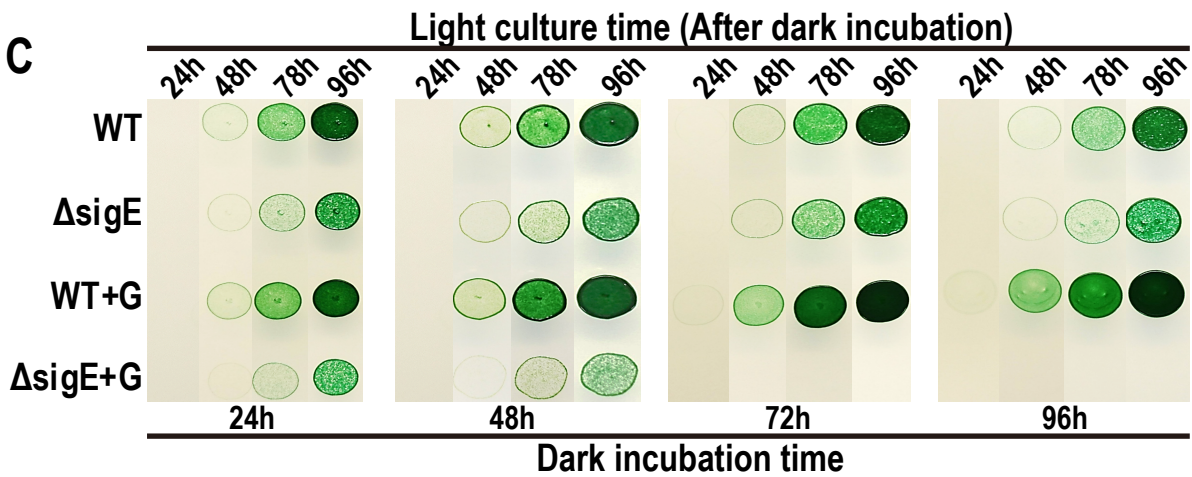


Figure 3

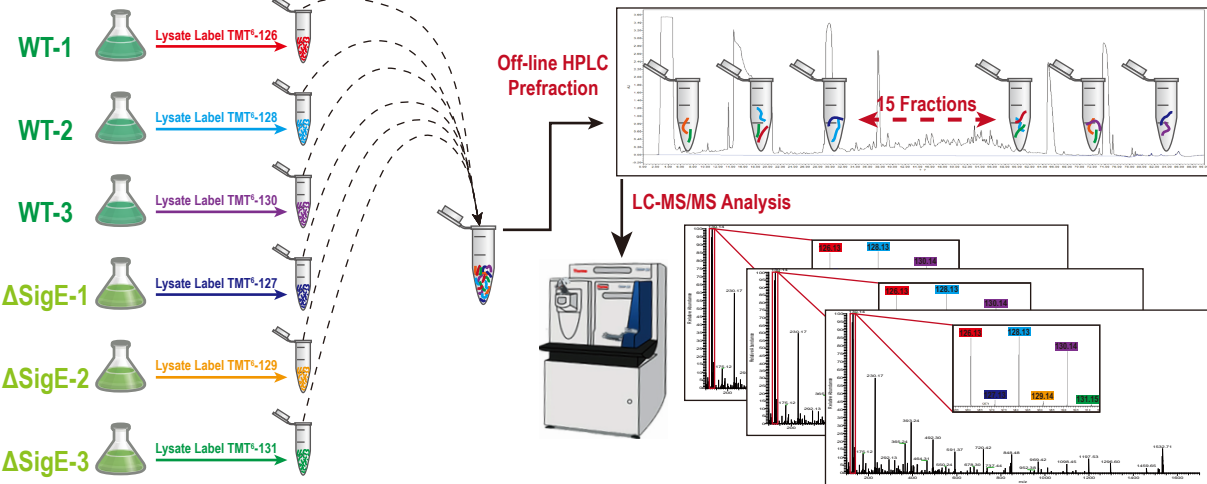
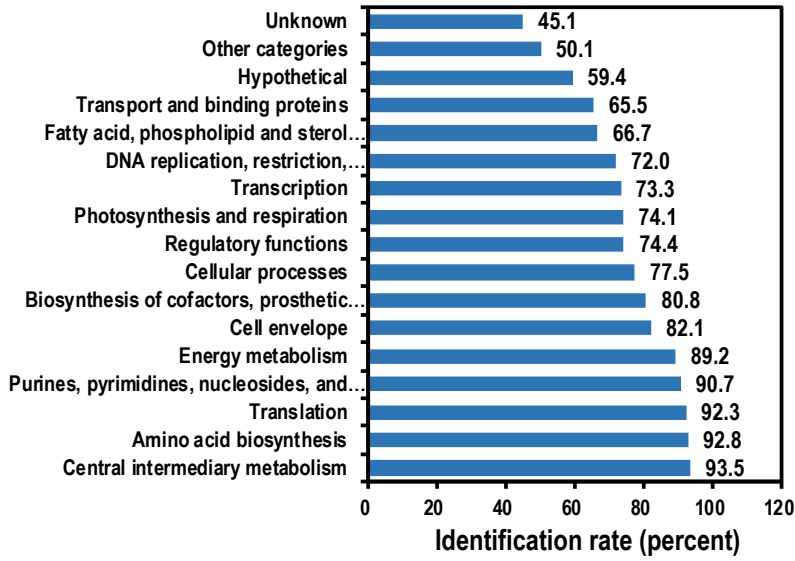
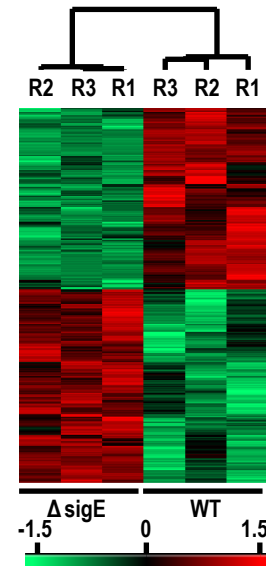


Figure 4

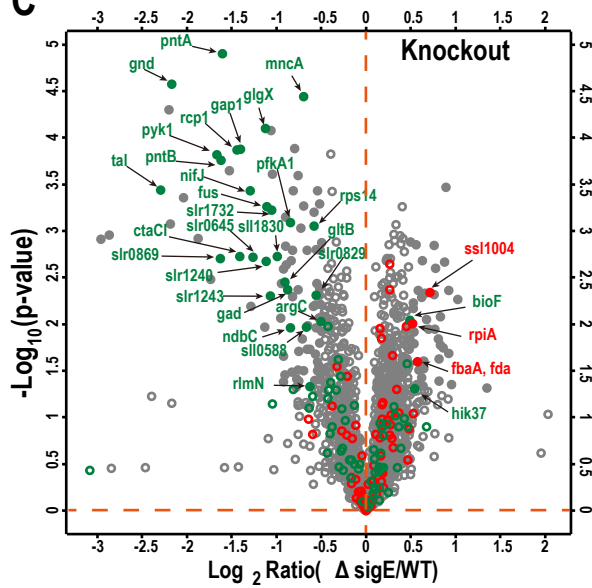
A



B



C



D

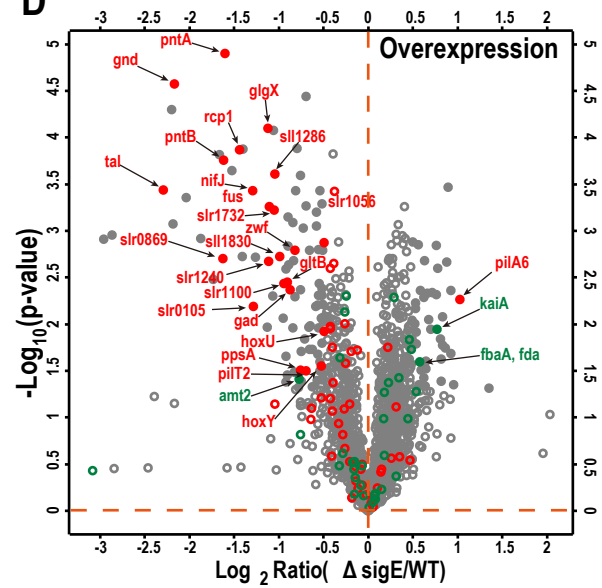


Figure 5

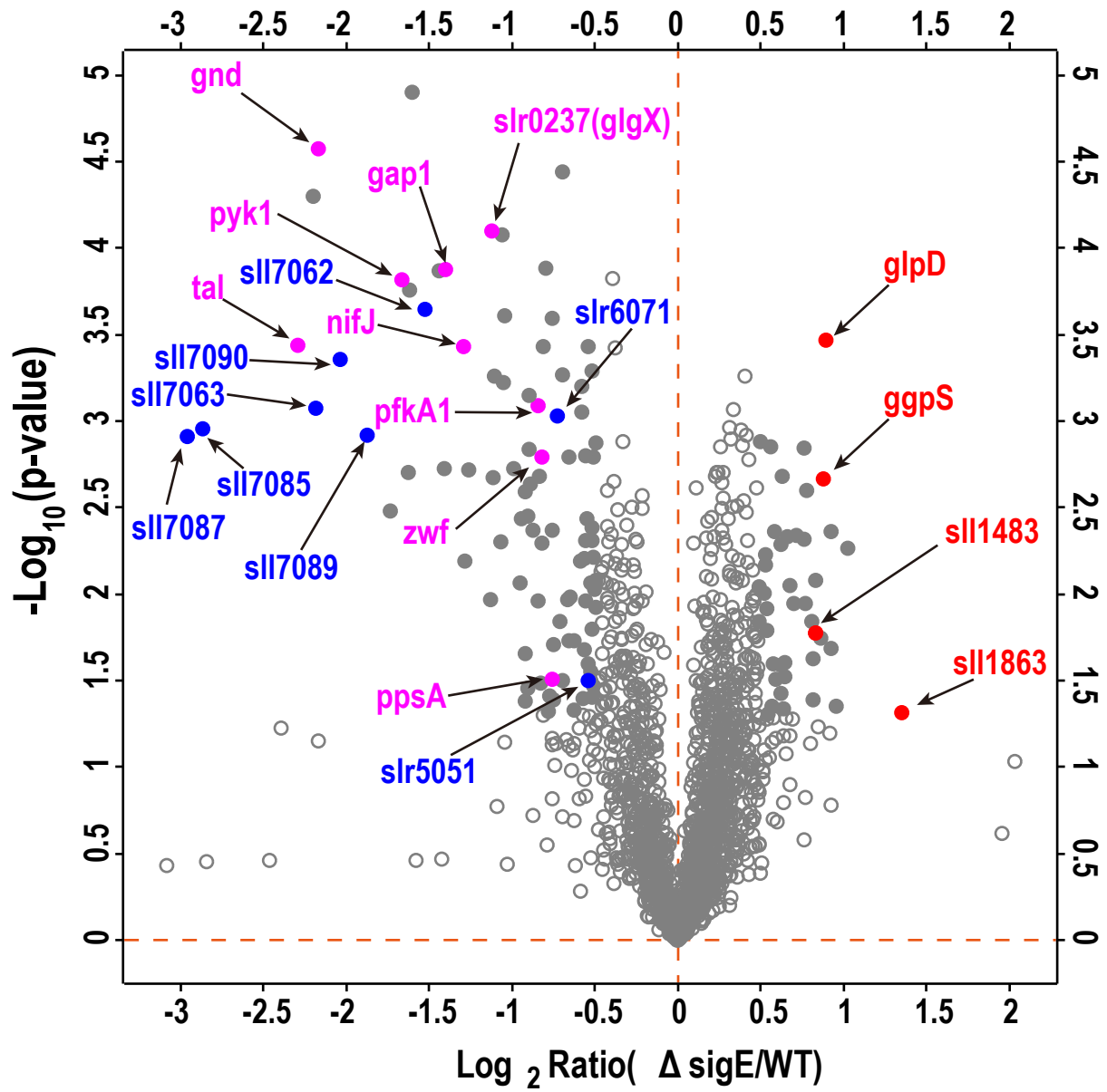


Figure 6

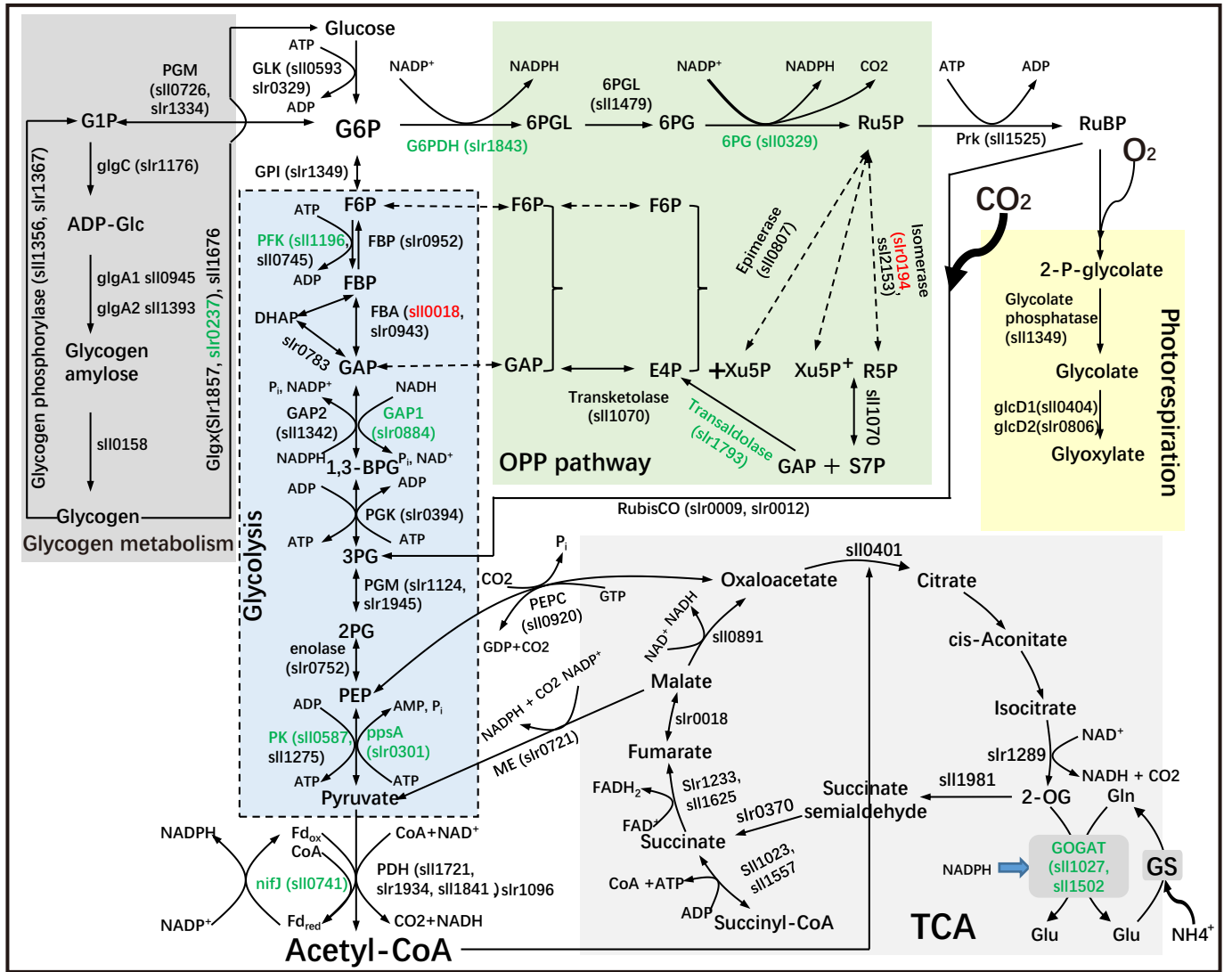
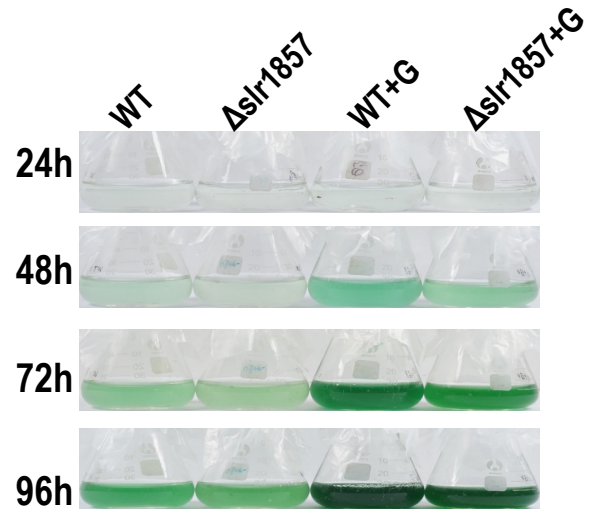
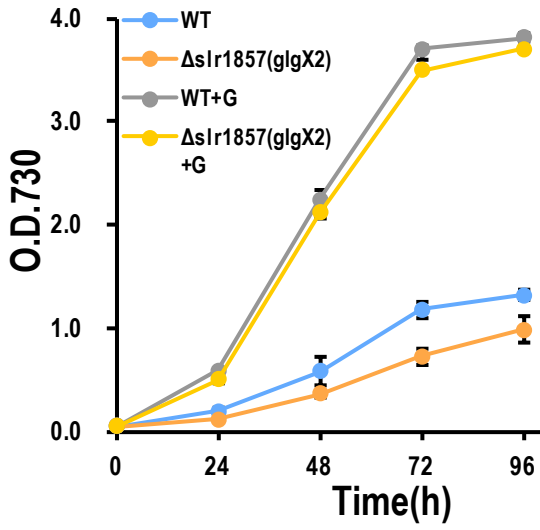
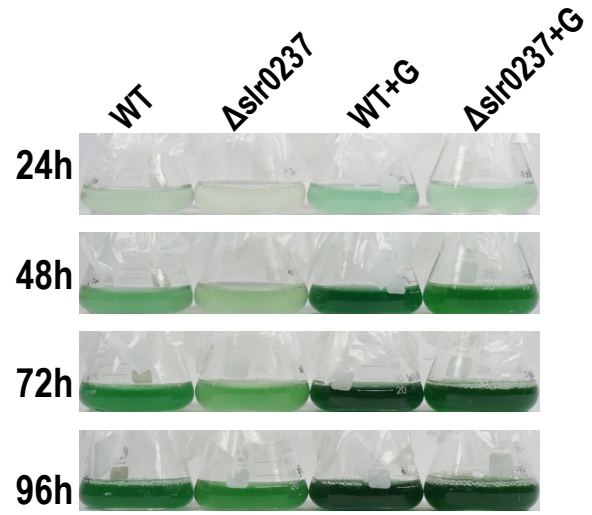
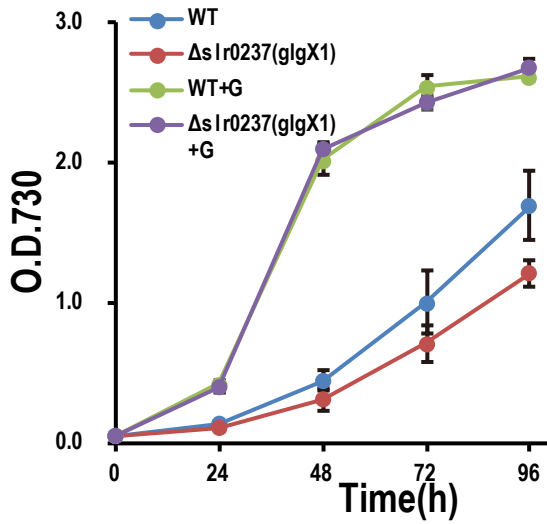


Figure 7

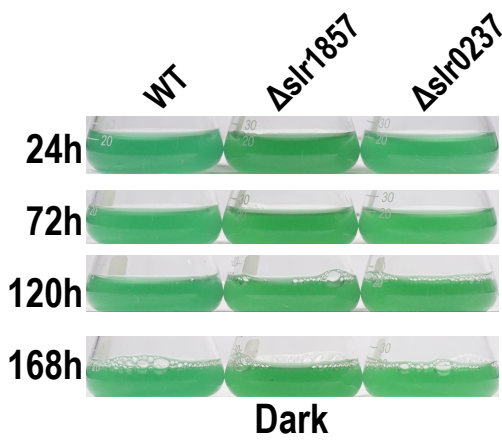
A



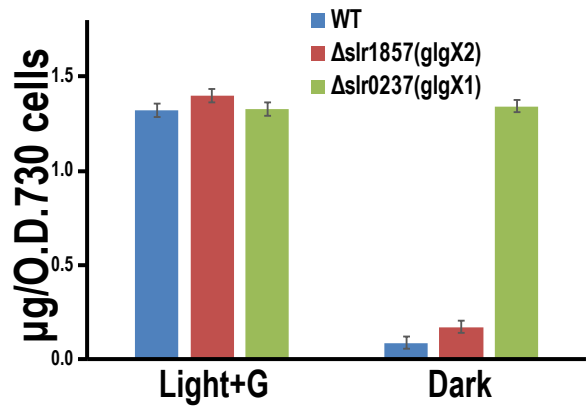
B



C

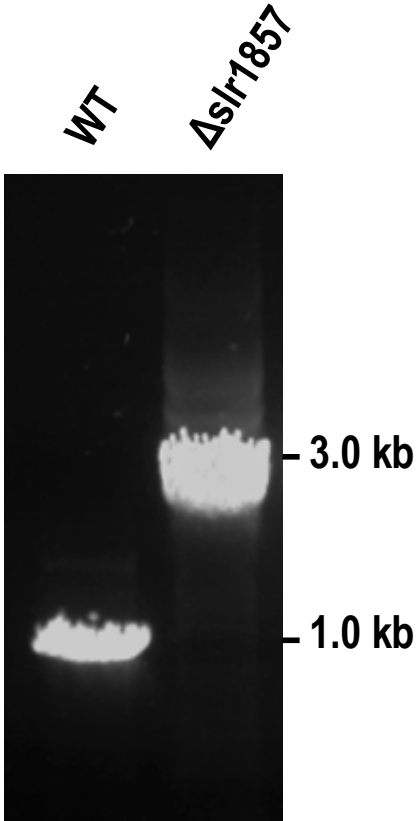


D

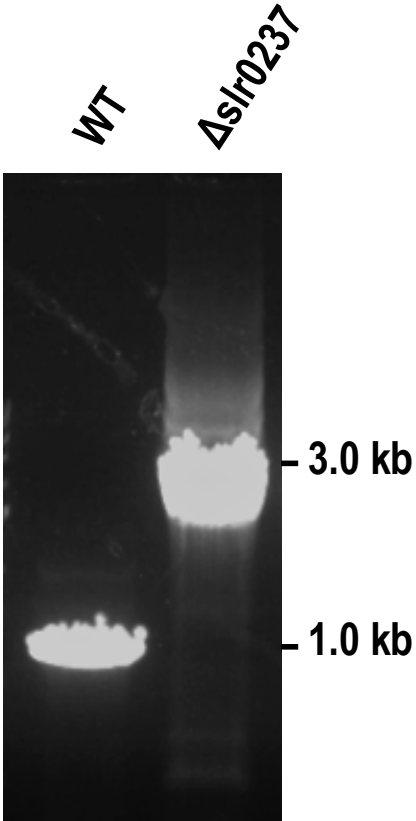


Supplemental Figure 1

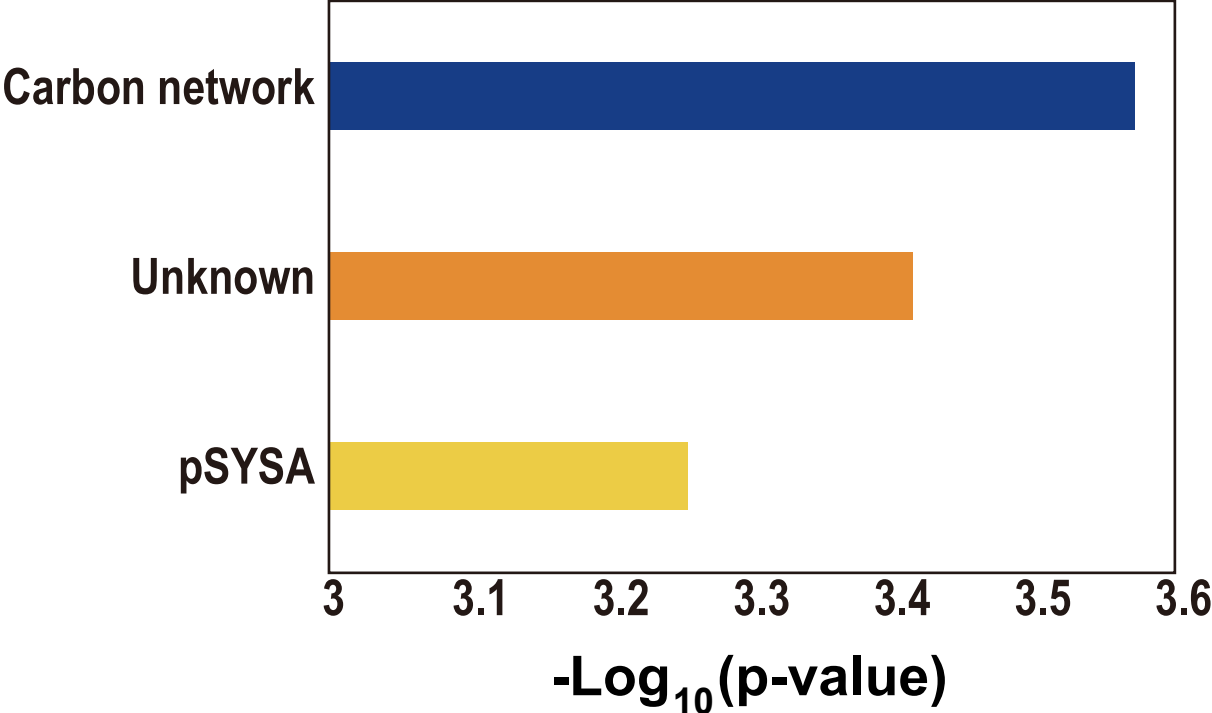
A



B



Supplemental Figure 2



Supplemental Figure 3

